Current Applied Physics 22 (2021) 43–49

Contents lists available at ScienceDirect

Current Applied Physics

journal homepage: www.elsevier.com/locate/cap

Nanosecond laser-induced reshaping of periodic silicon nanostructures

Phuong Thi Nguyen [a], Jina Jang [a], Seok-Min Kim [b], Taeseung Hwang [c], Junyeob Yeo [c], Costas P. Grigoropoulos [d], Jung Bin In [a,*]

[a] Soft Energy Systems and Laser Applications Laboratory, School of Mechanical Engineering, Chung-Ang University, Seoul, 06974, Republic of Korea
[b] Nano Micro Fabrication Technology Laboratory, School of Mechanical Engineering, Chung-Ang University, Seoul, 06974, Republic of Korea
[c] Novel Applied Nano Optics (NANO) Lab, Department of Physics, Kyungpook National University, Daegu, 41566, Republic of Korea
[d] Laser Thermal Laboratory, Department of Mechanical Engineering, University of California, Berkeley, CA, 94720, United States

ARTICLE INFO

Keywords:
Laser reshaping
Silicon nanostructure
Ablation
Self-assembly

ABSTRACT

We demonstrated the use of laser-induced reshaping to produce periodic silicon nanostructures (PSNs) with different geometries. Periodically located silicon nanostructures were preformed by dry etching of a silicon wafer covered with a monolayer of self-assembled polystyrene nanospheres. These PSNs were reshaped under ambient conditions by irradiation with two kinds of nanosecond lasers (532 nm and 355 nm). The effects of the irradiation parameters on the reshaped geometry were systematically investigated. Vertical growth of the irradiated PSNs resulted from the epitaxial deposition of rich silicon vapor during laser irradiation. However, the growth was limited even with higher laser fluence because of the nanoscale structure, the size of which is smaller than the melting depth induced by the nanosecond lasers. The reshaped PSNs displayed reflection spectra that are tunable by varying the characteristics of reshaping-laser input. This method offers a promising approach for the site-selective fabrication of optically tunable 3D nanostructures.

1. Introduction

Recently, periodic silicon nanostructures (PSNs), in forms of nanopillars, nanowires, nanocones, and nanotubes, have gained considerable attention of researchers owing to their unique physical properties and compatibility with micro/nano-fabrication processes that are well established in the modern semiconductor industry. In relation to their optical properties, many studies have demonstrated that Mie resonance is active in PSNs, which can be exploited for numerous applications including plasmonics [1], photonics [2–6], and photovoltaics [5,7,8]. Various fabrication methods have been proposed to obtain PSNs in a controlled manner. They include lithographic micro/nano-patterning by electron-beam writing, nanoimprinting, self-assembled nanosphere, and block copolymer, after which selective etching can be used to produce 3D PSNs [1,9,10].

The 3D PSNs offer a new dimension, especially in manipulating the optical properties of Si nanostructures. Although the aforementioned techniques can be used to fabricate PSNs with uniform geometries, the variety in 3D geometrical structure is limited. This pertains to the lack of controllability in the etching direction. The bottom-up building of PSNs that include techniques such as chemical vapor deposition growth of Si nanowires may be a plausible alternative, but it generally involves the use of high-temperature processes and foreign elements such as metal catalysts, which may affect the material integrity [11]. Sophisticated high-precision 3D nanoprinting system may enable true 3D nanofabrication [12–14], but this slow direct writing process is not suitable for large-scale production. Multiple patterning processes can be used to implement 3D geometry engineering; however, this is costly, complicated, and requires several precise steps [15,16].

In this respect, thermally induced reshaping of PSNs is a promising method that can be used for modifying the shape of PSNs and tuning their optical properties. This is because it requires simple heating of the structure up to a high temperature where the Si atoms at the surface become mobile. Thus, spontaneous dewetting induced by heat stands out as a facile and high-throughput method. For instance, Thompson et al. demonstrated the reshaping of a Si film into spherical or faceted particles, which cannot be produced by other conventional lithographic techniques [17]. Naffouti et al. presented a dewetting process to control the size, shape, and relative position of reshaped periodic silicon particles [18]. However, despite the excellent controllability of reshaped structure, these methods require long process time that may be more than several hours and tight ambiance control such as ultrahigh vacuum

* Corresponding author.
E-mail address: jbin@cau.ac.kr (J.B. In).

https://doi.org/10.1016/j.cap.2020.12.003
Received 20 July 2020; Received in revised form 24 November 2020; Accepted 8 December 2020
Available online 15 December 2020

conditions.

Besides, many researchers have proposed laser-induced reshaping of PSNs, which is a branch of thermal reshaping techniques and is a rapid and cost-effective method [6,19–21]. The photothermal interaction between laser and 3D PSNs can elevate the temperature of the irradiated PSNs high enough to induce thermal reshaping of the PSNs [22,23]. Moreover, it is possible to control the interaction time (generally from hundreds of femtoseconds to tens of milliseconds) using high-speed laser beam scanning or temporally modulated short pulse lasers, resulting in minimal chemical modification of the irradiated surface. Thus, ambient laser processing for reshaping the PSNs becomes possible. In addition, by choosing a short wavelength that allows short optical penetration into Si, laser irradiation can modify the surface structure without altering the bulk of the material [24]. Furthermore, the laser reshaping technique enables site-selective modification of PSNs by programmed laser irradiation [20,25], which is highly promising for applications in metasurface, structural color printing [21], and sensing devices.

Previous laser reshaping studies used the PSNs that were prepared on insulating substrates such as glass [20,25]. Laser-induced shape evolution from a flat Si surface to nanostructures has been demonstrated mostly for antireflection surface applications. This is a template-free method, but the generated silicon nanostructures are randomly arranged. Recently, Aouassa et al. demonstrated laser reshaping of 3D PSNs preformed on a Si wafer [19]. However, a continuous wave laser was used in their study, resulting in shape change driven by laser melting and the subsequent dewetting.

In this study, we report nanosecond laser-induced reshaping of the 3D PSNs that are preformed via etching of a silicon wafer covered with a self-assembled nanosphere template. Visible and ultraviolet (UV) nanosecond lasers were applied to the preformed PSNs. The vertical growth of the PSNs was observed, and we discuss its growth mechanism. The effects of laser irradiation parameters on the PSN geometry and the resulting optical characteristics were investigated.

2. Experimental section

Silicon template preparation. A *p*-type (100) Si wafer (dopant: boron, resistivity: 1–10 Ω cm) was cut into 1 × 1 cm^2 pieces. The Si pieces were first cleaned in a mixture solution of acetone, ethanol, and deionized water (1:1:1 in volume ratio) using a bath sonicator for 30 min. For complete removal of the remaining contaminants, the Si pieces were immersed in a Piranha solution containing H_2SO_4 (98 wt%) and H_2O_2 (30 wt%) in a volume ratio of 3:1, for 1 h at 80 °C. The cleaned Si was dried under a nitrogen atmosphere. Polystyrene (PS) nanosphere solution (0.8 μm in mean diameter, 10 wt% in solid concentration, Sigma-Aldrich) was coated onto the silicon substrate by using a spin coater (SPIN-1200D, MIDAS) for 60 s at a speed of 3000 rpm. The sample was then annealed at 65 °C in a vacuum oven (HQ-VDO27, CORETECH) to remove the excess solvent and enhance the adhesion between the deposited PS nanospheres and Si substrate.

The sample was etched using an inductively coupled plasma (ICP) etcher (ICP 380, Oxford System), which selectively removes Si faster than PS. The flow rates of the reactive ion etching (RIE) gases consisting of SF_6, O_2, and CHF_3 were 45, 5, and 50 SCCM, respectively. The mixture gas pressure was controlled to be 80 mTorr, and the plasma power was set to 150 W for 4 min. For the complete removal of the PS nanospheres, the sample was cleaned in ethanol and acetone mixture (1:1 in volume ratio) using a bath sonicator.

Laser irradiation. Two kinds of lasers were employed for the laser-induced reshaping of PSNs. A nanosecond laser (pulse duration: 6–9 ns, repetition rate: 20 Hz, Nano L200-20, Litron) was used for laser irradiation. This laser produced a laser beam with a fundamental wavelength of 1064 nm, and its frequency was doubled (wavelength: 532 nm) by using a second harmonic generation unit. A 5 × beam expander (Thorlabs) was installed in conjunction with an adjustable iris to enlarge the beam size and improve the beam shape. The laser beam was focused via an objective lens (5 × magnification, NA: 0.14, PAL-5, OptoSigma) and incident normally on the Si substrate. The diameter of the laser beam was measured to be approximately 50 μm based on the knife-edge method. All laser experiments were conducted under ambient conditions.

The other laser used was a UV nanosecond laser (pulse duration: 13.5 ns, repetition rate: 30 kHz, Poplar-355-3, Huaray). The laser beam was guided by a galvanometer mirror scanner (hurrySCAN II 10, SCANLAB), and it was focused onto a sample via an f-theta lens (f = 103 mm). The estimated beam size ($1/e^2$ diameter) was approximately 8 μm. Owing to the high repetition rate, the number of irradiated laser pulses was controlled by adjusting the scanning speed of the laser beam. For instance, when the scanning speed was 1 mm/s, the center area of the beam spot was exposed to 240 pulses. No evidence of heat accumulation was observed.

Characterization. The morphology and dimensions of the reshaped PSNs were investigated using a field-emission scanning electron microscope (FE-SEM, SIGMA, Carl Zeiss). Transmission electron microscopy (TEM, JEM-2100F) was carried out to inspect the lattice structure of the reshaped PSNs. The specimen used for TEM analysis was prepared by focused ion beam (FIB) milling (FEI-Nova Nanolab). The reflection spectra of the PSNs were measured using a spectroscopic reflectometer (ST5000-Auto200, K-MAC). This spectroscopic reflectometer was equipped with a white light source (50 W tungsten-halogen light source), a spectrometer (grating: 600 lines/nm, slit: 50 μm, resolution < 1.7 nm), a 2048-pixel charge-coupled device detector (K-MAC), and a 5 × objective lens (NA: 0.1, spot size: 40 μm). Light reflectance in the range of 400–800 nm wavelength was collected with the incident light normal to the sample surface.

3. Results and discussion

3.1. Templated laser growth of silicon nanopillars

Fig. 1a depicts the fabrication process of the templated PSNs and laser-induced reshaping of their structure. As shown in Fig. 1b, spin-coating of PS nanospheres onto a silicon substrate produced a hexagonal close-packed (hcp) monolayer of the nanospheres via self-assembly [26]. The PS nanosphere acted as a mask for the following RIE of the underlying silicon substrate. Fig. 1c shows the SEM image of the etched silicon substrate that features periodic arrangement. The shape of the unit structure is similar to that of a truncated cone (top diameter: ~350 nm, base diameter: 800 nm, and height: 450 nm), and this structure provided a designated site for laser-induced reshaping. When irradiated with 355 nm ns laser beam pulses, the initial PSNs were transformed to vertical nanopillar arrays, as shown in Fig. 1d. The SEM inspection revealed that the reshaped PSNs grew protruding higher than the initial level of the original PSNs (also see Fig. S1 in the supplementary material).

The production of nanoscale Si column/cone arrays from flat Si surface by the irradiation of repeated laser pulses has been demonstrated in many studies [27–30]. Nucleation of the structure growth sites was ascribed to capillary waves induced by the density difference between Si liquid melt and solid Si, as well as the light interaction with surface plasmon polariton waves. However, the arrangements of such growth sites are mostly irregular except in few cases where limited periodicity appeared only in a local area [31]. In contrast, our initial PSNs contained designated growth sites; thus, the periodicity of the reshaped PSNs was maintained.

The internal structure of the reshaped pillar was examined via TEM. A focused ion beam was used to prepare a thin cross-sectional sample for the TEM analysis. Fig. 2a and b shows the cross-sectional TEM images of the initial pillar and the reshaped nanopillar that was formed by the 355 nm laser pulses (fluence: 1.53 J cm^{-2}, scanning speed: 1 mm/s), respectively. Fig. 2c and d shows the high-resolution TEM image and selected-area electron diffraction pattern for region C marked in Fig. 2b,

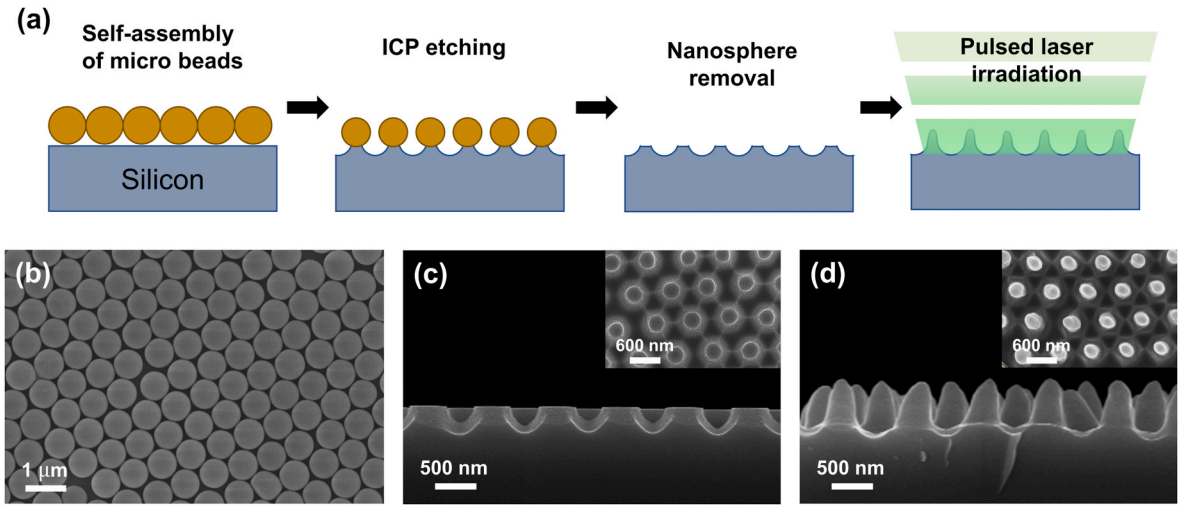

Fig. 1. (a) Schematic representation of the periodic silicon nanostructure fabrication and laser-induced reshaping of its structure. (b) Top-view SEM image of the self-assembled polystyrene nanosphere monolayer. (c) Side-view and top-view (inset) SEM images of the periodic silicon nanostructures after ICP etching and nanosphere removal. (d) Side-view and top-view (inset) SEM images of the laser-reshaped periodic silicon nanostructures (wavelength: 355 nm, fluence: 1.53 J cm^{-2}, and scanning speed: 1 mm/s). (For interpretation of the references to color in this figure legend, the reader is referred to the Web version of this article.)

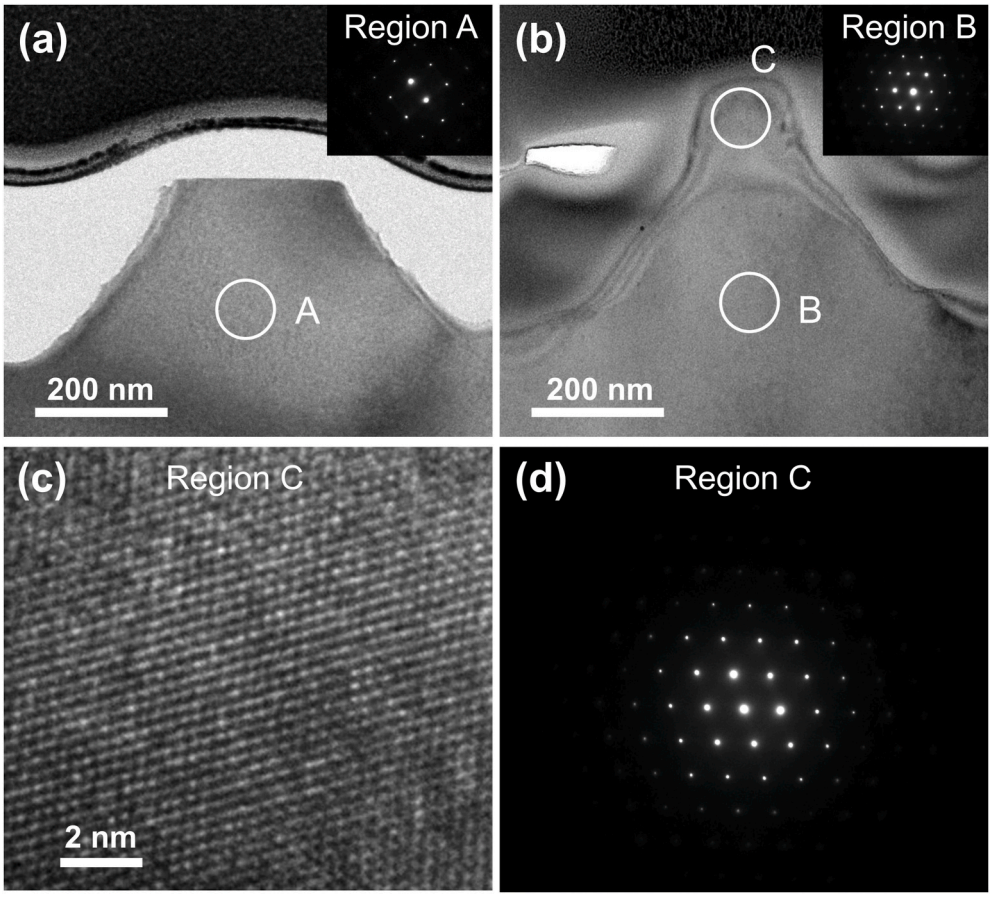

Fig. 2. TEM images of the initial Si structure (a) and the reshaped structure (b). The insets in Fig. 2a and b shows the electron diffraction pattern of region A and region B, respectively. (c) High-resolution TEM image of the crystal lattice of region C. (d) Electron diffraction pattern of region C.

respectively. These figures indicate that the Si in the growth region C is single crystalline with no grain boundaries [32]. Furthermore, the selected-area diffraction patterns of regions C and B (Fig. 2d and the inset of Fig. 2b, respectively) reveal that the structure grew epitaxially based on the underlying Si substrate. A thin oxide surface layer could hinder the epitaxial deposition of silicon atoms, but our results suggest that the oxide layer was ablated by the high-intensity laser pulse [33].

3.2. Effects of laser irradiation parameters

The effect of the laser irradiation parameters on the geometry of the reshaped structure was investigated. Fig. 3 shows the side-view SEM images of the Si structures reshaped by the 532 nm ns laser. Fig. 3a–d shows the morphological change caused by different laser fluences (from 0.5 J cm^{-2} to 1.2 J cm^{-2}, common pulse number: 300). Fig. 3a shows that at low fluence, a single nanopillar structure was produced from the top of each truncated cone structure. At higher fluences (Fig. 3b–d), the degree of reshaping was larger, owing to the increased melting depth. At the highest fluence (1.4 J cm^{-2}), the silicon sample surface was flattened owing to the complete melting and ablation of the nanostructure (see Fig. S2a in the supplementary material). Fig. 3e–h shows the evolutionary change in the geometry of the PSNs by repeated irradiation of laser pulses (from 100 to 900 pulses) at a fixed fluence (1.0 J cm^{-2}). The initial truncated cone structure changed into a columnar structure that was based on a trace of the initial structure. As shown in Figs. 3g and 600 pulses caused serious collapse of the Si columns. At a much larger number of pulses (900 pulses), the PSNs reduced in size, and their surfaces were covered with debris-like materials.

To investigate the effect of laser wavelength on the Si structure, the original Si structure was scanned with the UV nanosecond laser that has a shorter wavelength (355 nm) than the abovementioned nanosecond laser. The effects of different laser fluences and pulse numbers on the reshaping of the PSNs were also investigated. Fig. 4a–d shows side-view SEM images of the reshaped PSNs obtained in a fluence range of 1.13 J cm^{-2} to 1.92 J cm^{-2}. Similar to the 532 nm laser samples, the initial truncated cone structures were reshaped into nanopillars. Compared with the PSNs reshaped by the 532 nm laser, these reshaped PSNs exhibited more uniform geometry with a vertical alignment up to the fluence of 1.53 J cm^{-2}. For higher fluences, the nanopillars became shorter than the initial size because of the ablative removal of Si, and the nanopillars turned into nanocones with sharp tips (see Fig. S2b in the supplementary material).

The morphologies of the PSNs reshaped with the 355 nm laser were more uniform than those reshaped with the 532 nm laser. The orientations of the columns were more vertically aligned to the substrate. The columns of the PSNs reshaped with the 355 nm laser were terminated with sharp tips, whereas necks were observed below the blunt tips of the PSNs reshaped by the 532 nm laser. These differences can be attributed to shorter optical penetration (~10 nm) of the 355 nm laser that results in a smaller melt depth (or causes lesser thermal effect on the structure bulk) when compared with that (~1 μm) of the 532 nm laser [34]. For the same reason, the PSNs reshaped by the 532 nm laser collapsed at high fluences, as shown in Fig. 3. The different optical penetration depths between the two lasers were further confirmed by a finite-difference time-domain (FDTD) simulation (Fig. S3 in the supplementary material).

Fig. 5 shows the change in height of the PSN samples according to different laser fluences (Fig. 5a) and pulse numbers (Fig. 5b) for the 532 nm and 355 nm ns lasers. The height of the individual Si structures is defined as the distance from the deepest base to the top end of the structure. The heights were measured from the pillars reshaped within the beam width (50 μm for the 532 nm laser and 8 μm for the 355 nm laser). The variation in diameter was not evaluated because of the tapered shape. Since laser-induced reshaping occurred preferentially in the initial PSNs, the density of the PSNs was maintained except in situations where a high-fluence laser beam ablated the structures. For both lasers, the average height of the Si nanopillars initially increased with laser fluence, and it peaked at maximum values of 820 nm at ~1 J cm^{-2} for the 532 nm laser and 795 nm at ~1.53 J cm^{-2} for the 355 nm laser. However, at higher laser fluences, the height considerably decreased because the ablative removal of Si from the nanopillar tips was faster than the laser-induced growth. This result is consistent with other experimental studies [32,35]. As shown in Fig. 5b, a similar trend was observed for the effect of laser pulse number on the height [35,36]. The maximum heights were obtained at 400 pulses for the 532 nm laser and 240 pulses for the 355 nm laser. We believe that this is attributable to evolutionary change in the PSN morphology (Fig. 3) with repeated irradiation of laser pulses. That is, the PSNs were gradually changed into the structures that were less active in the laser-induced growth.

Various mechanisms have been proposed in previous studies to account for the formation of columnar Si structures on Si wafers by repeated pulsed laser irradiation [28,32,37]. Among them, Pedraza et al. suggested a vapor-liquid-solid growth mechanism to explain the growth of Si microcolumns that longitudinally extended to tens of micrometers [28]. They observed random generation of growth nuclei near cracks and pits in the initial stage of growth. These nuclei protruded from the substrate and continued growing aligned to the direction of the incident laser beam. When the Si structure was irradiated with a laser, the column tip melted and accommodated the intense flux of the silicon-rich vapor produced by the ablation of the surface regions between columns. As a result, the Si structure grew longitudinally. It has been experimentally demonstrated that not only excimer nanosecond lasers but also visible nanosecond lasers enabled such growth [32,37].

However, as shown in Fig. 5a, the length of our reshaped PSNs was below 1 μm, although the growth mode was active as shown in Fig. S1. We suggest that the discrepancy possibly originates from the high

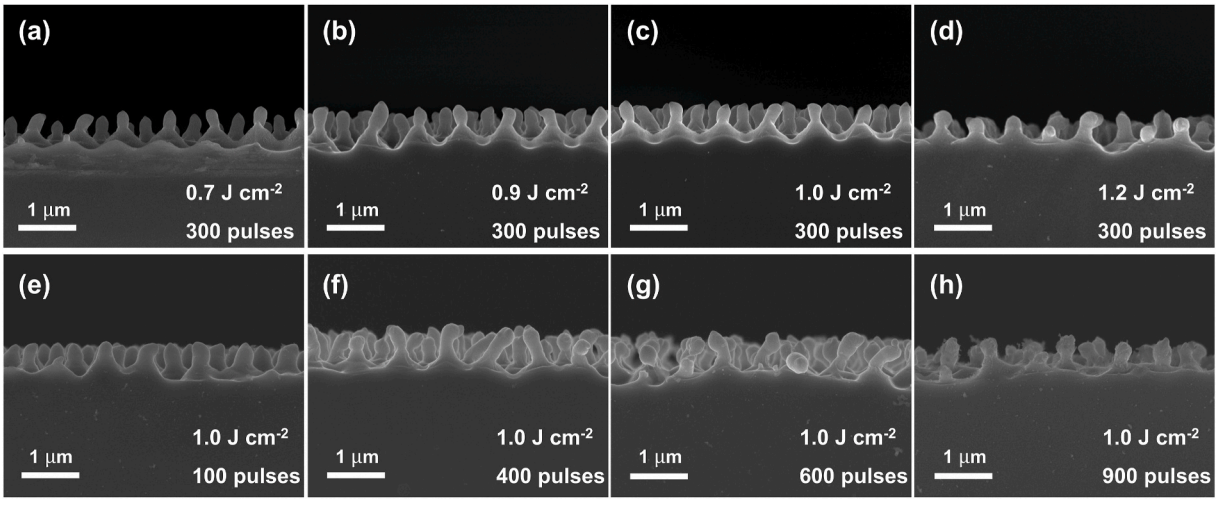

Fig. 3. Side-view SEM images of the reshaped silicon nanostructures irradiated with 300 pulses of the 532 nm ns laser beam at different laser fluences (a–d) and with different numbers of the beam pulses at a fixed fluence of 1.0 J cm^{-2} (e–h).

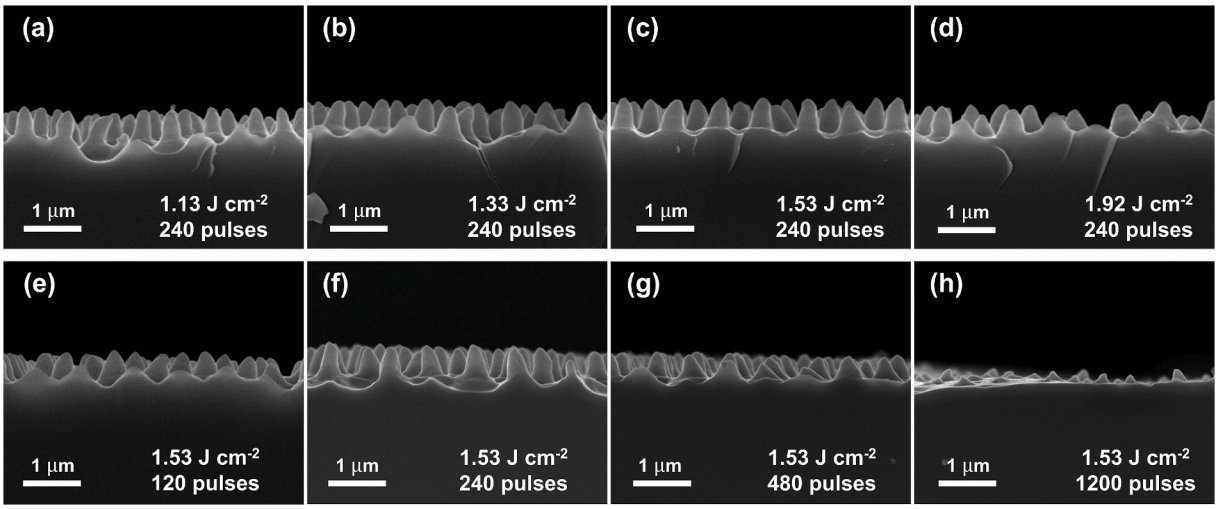

Fig. 4. Side-view SEM images of the reshaped silicon nanostructures irradiated at a scanning speed of 1 mm/s with the 355 nm UV laser beam at different laser fluences (a–d) and with different numbers of the beam pulses at a fixed fluence of 1.53 J cm^{-2} (e–h).

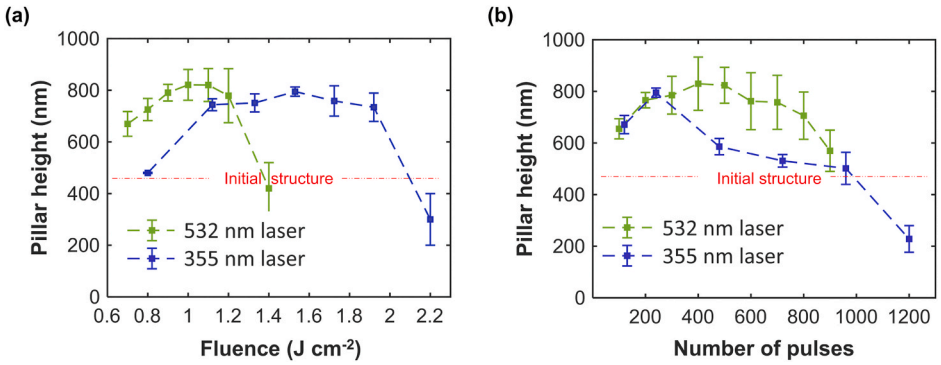

Fig. 5. Change in PSN height with laser fluence (fixed number of pulses: 300 for the 532 nm laser and 240 for the 355 nm laser) (a) and the number of pulses (fixed fluence: 1 J cm^{-2} for the 532 nm laser and 1.53 J cm^{-2} for the 355 nm laser) (b).

number density of our templated growth sites when compared with previous studies. If the density of the growth site is too high to be sufficiently provided with Si under a limited flux of ablated Si, elongation will not proceed. The Si flux to the growth tip possibly decreases in accordance with the evolutionary reshaping of the structure [36,38]. Moreover, part of the growth tip was also ablated during the laser irradiation. Thus, as shown in Fig. 5, the nanopillar could be shortened because of the faster ablation of the growth tip than the Si influx. Increased laser fluence may increase the Si flux, which enables extended growth. Pedraza et al. demonstrated such elongated growth of Si microcolumns at a UV laser (wavelength: 248 nm) fluence of 2.7–3.3 J cm^{-2} [28]. However, as discussed by Lowndes et al. the molten tip size that is comparable to melt depth is larger than 1 μm [30], which would destroy the nanoscale feature of our PSNs. The growth of Si nanopillars could be hampered by a thick oxide layer that could be formed by air, but this is not the cause of the retarded growth as shown in the TEM image (Fig. 2).

The shape modification of PSNs causes change in the reflection characteristics, which has been widely investigated by many studies related to nanophotonics [4,25,39–41]. The PSN samples irradiated

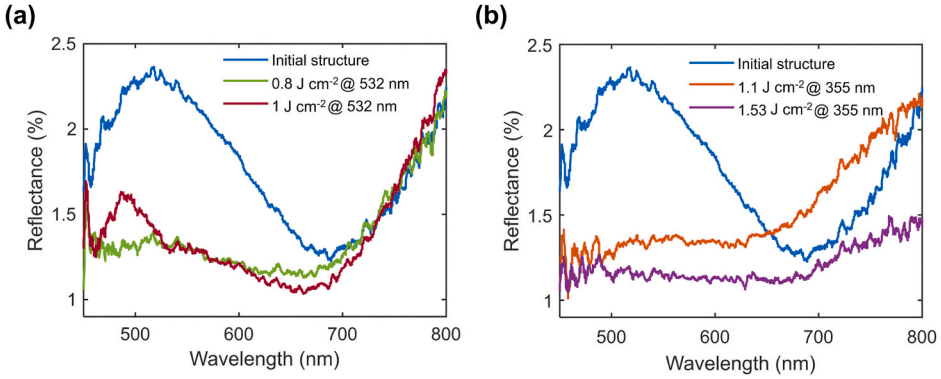

Fig. 6. Reflection spectra of the initial structure and the structures of the PSNs reshaped by the 532 nm laser (a) and 355 nm laser (b).

with the lasers at different fluences were used to investigate the effect of the laser fluence on the reflection spectrum. Fig. 6 shows the reflectance spectra of the initial PSNs and the reshaped PSNs at 0.8 and 1 J cm^{-2} with the 532 nm laser, and at 1.1 and 1.53 J cm^{-2} with the 355 nm laser. For the wavelength range of 450–800 nm, all PSNs exhibited low reflectances (less than 2.5%), which can be attributed to a gradient refractive index between air and the base surface [42]. The reflection characteristics of the reshaped PSNs were significantly different from those of the initial PSNs. For relatively short visible wavelengths (450–600 nm), the reflectance markedly decreased below ~1.7% as a result of laser reshaping of the PSNs. This is consistent with previous studies that demonstrated a decrease in reflectance with an increase in the length of the nanopillar, nanocone, or nanowire Si structures [43, 44]. Moreover, the tips of the reshaped PSNs became sharp and thus enabled smooth change in the refractive index at the air-PSN interface, which is beneficial to the antireflection performance.

The PSNs irradiated with different lasers or with the same laser but different laser fluences also showed distinct spectral responses. As shown in Fig. 6a, a reflection peak was observed near 480 nm for the PSNs reshaped by the 532 nm laser at 1 J cm^{-2}, whereas no obvious peaks were observed for the PSNs reshaped at 0.8 J cm^{-2}. The characteristics of these spectra were consistently observed from different spots. For the PSNs irradiated with the 355 nm laser, multiple absorption peaks were observed in the wavelength range of 450–500 nm (Fig. 6b). The PSNs irradiated at 1.53 J cm^{-2} exhibited a lower reflectance when compared with the PSNs irradiated at 1.1 J cm^{-2}. These results substantiate the tailoring of PSN optical responses enabled by nanosecond lasers.

4. Conclusions

In conclusion, we have demonstrated that the nanosecond laser reshaping method can be used to modify the 3D geometry of PSNs and tailor their optical reflectance. As a result of the repeated laser pulse inputs, the initial PSNs evolved into nanopillars. For the 355 nm UV laser irradiation, the pillar structure maintained vertical alignment, whereas the PSNs were collapsed by the 532 nm visible laser because of large melting depth. The increased laser fluence and laser pulse number elongated the pillar structure to a certain degree. However, the growth length was limited below ~500 nm because of the lack of ablated Si vapor. This nanoscale structure modification led to change in the spectral characteristics of PSN reflectance. Our method can implement site-selective reshaping of PSNs. Therefore, it can be potentially applied to optical data storage, metasurfaces [41], sensors, and anti-reflection surfaces [45].

Declaration of competing interest

The authors declare that they have no known competing financial interests or personal relationships that could have appeared to influence the work reported in this paper.

Acknowledgments

This research was supported by the Chung-Ang University Research Grants in 2019; and the National Research Foundation of Korea (NRF) grant funded by the Korea government (MSIT) (No. NRF-2019R1F1A1059281).

Appendix A. Supplementary data

Supplementary data to this article can be found online at https://doi.org/10.1016/j.cap.2020.12.003.

References

[1] S. Kasani, K. Curtin, N. Wu, A review of 2D and 3D plasmonic nanostructure array patterns: fabrication, light management and sensing applications, Nanophotonics 8 (2019) 2065–2089.
[2] P. Bettotti, M. Cazzanelli, L.D. Negro, B. Danese, Z. Gaburro, C.J. Oton, G. V. Prakash, L. Pavesi, Silicon nanostructures for photonics, J. Phys. Condens. Matter 14 (2002) 8253–8281.
[3] R. Yan, D. Gargas, P. Yang, Nanowire photonics, Nat. Photon. 3 (2009) 569.
[4] C.S. Park, V.R. Shrestha, W. Yue, S. Gao, S.S. Lee, E.S. Kim, D.Y. Choi, Structural color filters enabled by a dielectric metasurface incorporating hydrogenated amorphous silicon nanodisks, Sci. Rep. 7 (2017) 2556.
[5] F. Priolo, T. Gregorkiewicz, M. Galli, T.F. Krauss, Silicon nanostructures for photonics and photovoltaics, Nat. Nanotechnol. 9 (2014) 19–32.
[6] S.V. Makarov, A.S. Zalogina, M. Tajik, D.A. Zuev, M.V. Rybin, A.A. Kuchmizhak, S. Juodkazis, Y. Kivshar, Light-induced tuning and reconfiguration of nanophotonic structures, Laser Photon. Rev. 11 (2017).
[7] T. Song, S.-T. Lee, B. Sun, Silicon nanowires for photovoltaic applications: the progress and challenge, Nanomater. Energy 1 (2012) 654–673.
[8] N. Fukata, T. Subramani, W. Jevasuwan, M. Dutta, Y. Bando, Functionalization of silicon nanostructures for energy-related applications, Small 13 (2017).
[9] H. Li, J. Niu, G. Wang, E. Wang, C. Xie, Direct production of silicon nanostructures with electrochemical nanoimprinting, ACS Applied Electronic Materials 1 (2019) 1070–1075.
[10] M. Fang, H. Lin, H.Y. Cheung, F. Xiu, L. Shen, S. Yip, E.Y. Pun, C.Y. Wong, J.C. Ho, Polymer-confined colloidal monolayer: a reusable soft photomask for rapid wafer-scale nanopatterning, ACS Appl. Mater. Interfaces 6 (2014) 20837–20841.
[11] V. Schmidt, J.V. Wittemann, U. Gösele, Growth, thermodynamics, and electrical properties of silicon nanowires, Chem. Rev. 110 (2010) 361–388.
[12] Q. Li, D. Grojo, A.-P. Alloncle, B. Chichkov, P. Delaporte, Digital laser micro- and nanoprinting, Nanophotonics 8 (2018) 27–44.
[13] A. Vyatskikh, S. Delalande, A. Kudo, X. Zhang, C.M. Portela, J.R. Greer, Additive manufacturing of 3D nano-architected metals, Nat. Commun. 9 (2018).
[14] L. Hirt, A. Reiser, R. Spolenak, T. Zambelli, Additive manufacturing of metal structures at the micrometer scale, Adv. Mater. 29 (2017).
[15] A.C. Fischer, L.M. Belova, Y.G.M. Rikers, B.G. Malm, H.H. Radamson, M. Kolahdouz, K.B. Gylfason, G. Stemme, F. Niklaus, 3D free-form patterning of silicon by ion implantation, silicon deposition, and selective silicon etching, Adv. Funct. Mater. 22 (2012) 4004–4008.
[16] Y. Zhao, E. Berenschot, H. Jansen, N. Tas, J. Huskens, M. Elwenspoek, Multi-silicon ridge nanofabrication by repeated edge lithography, Nanotechnology 20 (2009) 315305.
[17] C.V. Thompson, Solid-state dewetting of thin films, Annu. Rev. Mater. Res. 42 (2012) 399–434.
[18] M. Naffouti, T. David, A. Benkouider, L. Favre, A. Delobbe, A. Ronda, I. Berbezier, M. Abbarchi, Templated solid-state dewetting of thin silicon films, Small 12 (2016) 6115–6123.
[19] M. Aouassa, E. Mitsai, S. Syubaev, D. Pavlov, A. Zhizhchenko, I. Jadli, L. Hassayoun, G. Zograf, S. Makarov, A. Kuchmizhak, Temperature-feedback direct laser reshaping of silicon nanostructures, Appl. Phys. Lett. 111 (2017).
[20] J. Berzinš, S. Indrišiūnas, S. Fasold, M. Steinert, O. Žukovskaja, D. Cialla-May, P. Gečys, S.M.B. Bäumer, T. Pertsch, F. Setzpfandt, Laser-induced spatially-selective tailoring of high-index dielectric metasurfaces, Optic Express (2020) 28.
[21] X. Zhu, C. Vannahme, E. Hojlund-Nielsen, N.A. Mortensen, A. Kristensen, Plasmonic colour laser printing, Nat. Nanotechnol. 11 (2016) 325–329.
[22] B. Xiang, D.J. Hwang, J.B. In, S.G. Ryu, J.H. Yoo, O. Dubon, A.M. Minor, C. P. Grigoropoulos, In situ TEM near-field optical probing of nanoscale silicon crystallization, Nano Lett. 12 (2012) 2524–2529.
[23] J.B. In, B. Xiang, D.J. Hwang, S.G. Ryu, E. Kim, J.H. Yoo, O. Dubon, A.M. Minor, C. P. Grigoropoulos, Generation of single-crystalline domain in nano-scale silicon pillars by near-field short pulsed laser, Appl. Phys. Mater. Sci. Process 114 (2014) 277–285.
[24] M.S. Brown, C.B. Arnold, Fundamentals of laser-material interaction and application to multiscale surface modification, in: K. Sugioka, M. Meunier, A. Piqué (Eds.), Laser Precision Microfabrication, Springer Berlin Heidelberg, Berlin, Heidelberg, 2010, pp. 91–120.
[25] L.T. Wan, Y. Rho, W. Shou, S. Hong, K. Kato, M. Eliceiri, M. Shi, C. P. Grigoropoulos, H. Pan, C. Carraro, D.F. Qi, Programming nanoparticles in multiscale: optically modulated assembly and phase switching of silicon nanoparticle array, ACS Nano 12 (2018) 2231–2241.
[26] J. Chen, P. Dong, D. Di, C. Wang, H. Wang, J. Wang, X. Wu, Controllable fabrication of 2D colloidal-crystal films with polystyrene nanospheres of various diameters by spin-coating, Appl. Surf. Sci. 270 (2013) 6–15.
[27] S.I. Dolgaev, S.V. Lavrishev, A.A. Lyalin, A.V. Simakin, V.V. Voronov, G.A. Shafeev, Formation of conical microstructures upon laser evaporation of solids, Applied Physics A Materials Science & Processing 73 (2001) 177–181.
[28] A.J. Pedraza, J.D. Fowlkes, D.H. Lowndes, Silicon microcolumn arrays grown by nanosecond pulsed-excimer laser irradiation, Appl. Phys. Lett. 74 (1999) 2322–2324.
[29] S. Magdi, J. El-Rifai, M.A. Swillam, One step fabrication of Silicon nanocones with wide-angle enhanced light absorption, Sci. Rep. 8 (2018).
[30] D.H. Lowndes, J.D. Fowlkes, A.J. Pedraza, Early stages of pulsed-laser growth of silicon microcolumns and microcones in air and SF6, Appl. Surf. Sci. 154–155 (2000) 647–658.

[31] B.K. Nayak, K.Y. Sun, C. Rothenbach, M.C. Gupta, Self-organized 2D periodic arrays of nanostructures in silicon by nanosecond laser irradiation, Appl. Optic. 50 (2011) 2349–2355.
[32] J.W. Yan, J. Noguchi, Y. Terashi, Fabrication of single-crystal silicon micro pillars on copper foils by nanosecond pulsed laser irradiation, CIRP Ann. - Manuf. Technol. 66 (2017) 253–256.
[33] M.J. Godbole, D.H. Lowndes, A.J. Pedraza, Excimer-laser ablation and activation of siox and siox-ceramic couples for electroless copper plating, Appl. Phys. Lett. 63 (1993) 3449–3451.
[34] N. Palina, T. Mueller, S. Mohanti, A.G. Aberle, Laser assisted boron doping of silicon wafer solar cells using nanosecond and picosecond laser pulses, in: 2011 37th IEEE Photovoltaic Specialists Conference, 2011, 002193-002197.
[35] S. Magdi, J. El-Rifai, M.A. Swillam, Lithography-free fabrication of crystalline silicon nanowires using amorphous silicon substrate for wide-angle energy absorption applications, ACS Appl. Nano Mater. 1 (2018) 2990–2996.
[36] A. Djemaa, N. Gabouze, C. Yaddadene, Y. Belaroussi, T. Kerdja, M. Kechouane, H. Menari, A.Y. Khereddine, Fabrication and characterization of silicon pillars formed by nanosecond pulsed excimer laser in vacuum, Surf. Interface Anal. 42 (2010) 1295–1298.
[37] S.I. Dolgaev, S.V. Lavrishev, A.A. Lyalin, A. Simakin, V.V. Voronov, G.A. Shafeev, Formation of conical microstructures upon laser evaporation of solids, Appl. Phys. Mater. Sci. Process 73 (2001) 177–181.
[38] Y. Belaroussi, T. Kerdja, C. Yaddadene, A. Djemaa, A. Keffous, N. Gabouze, Early stages of nanosecond pulsed-laser growth of silicon pillars in vacuum, J. Cryst. Growth 337 (2011) 20–23.
[39] X. Xu, Q. Yang, N. Wattanatorn, C. Zhao, N. Chiang, S.J. Jonas, P.S. Weiss, Multiple-patterning nanosphere lithography for fabricating periodic three-dimensional hierarchical nanostructures, ACS Nano 11 (2017) 10384–10391.
[40] S.E. Cheon, H.S. Lee, J. Choi, A.R. Jeong, T.S. Lee, D.S. Jeong, K.S. Lee, W.S. Lee, W.M. Kim, H. Lee, I. Kim, Fabrication of parabolic Si nanostructures by nanosphere lithography and its application for solar cells, Sci. Rep. 7 (2017) 7336.
[41] I. Staude, J. Schilling, Metamaterial-inspired silicon nanophotonics, Nat. Photon. 11 (2017) 274–284.
[42] J.G. Cai, L.M. Qi, Recent advances in antireflective surfaces based on nanostructure arrays, Mater Horiz 2 (2015) 37–53.
[43] Q. Fan, Z. Wang, Y. Cui, Optimal design of an antireflection coating structure for enhancing the energy-conversion efficiency of a silicon nanostructure solar cell, RSC Adv. 8 (2018) 34793–34807.
[44] Y. Xing, K. Zhang, J. Zhao, P. Han, Z. Yang, Y. Yuan, Q. Ding, Antireflection and absorption properties of silicon parabolic-shaped nanocone arrays, Optik 128 (2017) 133–138.
[45] J. Cai, L. Qi, Recent advances in antireflective surfaces based on nanostructure arrays, Mater Horiz 2 (2015) 37–53.